Hindawi
Geofluids
Volume 2022, Article ID 7851201, 15 pages
https://doi.org/10.1155/2022/7851201

Research Article

On the Dynamic Mechanical Behaviors of a Fault Unwelded Bimrock Exposed to Freeze-Thaw-Fatigue Loads: A Lab-Scale Testing

Yu Wang,[1,2] **Hongjian Wang**,[2] **Sun Tao**,[1] **and Xuefeng Yi**[1]

[1]*Beijing Key Laboratory of Urban Underground Space Engineering, Department of Civil Engineering, School of Civil & Resource Engineering, University of Science & Technology Beijing, Beijing 100083, China*
[2]*Key Laboratory of Geological Environment Intelligent Monitoring and Disaster Prevention and Control of Henan Province, North China University of Water Resources and Electric Power, Zhengzhou 450045, China*

Correspondence should be addressed to Yu Wang; wyzhou@ustb.edu.cn and Hongjian Wang; whjian_ncuw@126.com

Received 19 January 2022; Accepted 9 March 2022; Published 30 March 2022

Academic Editor: Zhiwei Zhou

This work is aimed at investigating the mechanical behaviors of a fault unwelded bimrock subjected to coupled freeze-thaw (FT) and fatigue loads. The influence of FT cycle on rock strength, deformation, damage evolution, and failure morphology was detailed investigated. The testing results show that the soil-rock interface is sensitive to freeze-thaw condition. Interface damage and cracking contribute a lot to sample strength, volumetric deformation, and damage evolution. In addition, a sudden increase of stress amplitude results in the increase of damage, afterwards, the coupling degree of bimrock improves with the increase of loading cycles. A coupling freeze-thaw and mechanical damage evolution model was proposed using the damage index defined by ultrasonic velocity and axial strain. It is found that the evolution trend of the model is strongly related to the previous freeze-thaw damage. Moreover, failure mode of bimrock changes from shear failure to bulging failure with increasing FT cycles. The failure process of bimrock is the rearrangement of the fine soil particles and rock blocks, the soil matrix and rock block bear axial cyclic loads by their interactions.

1. Introduction

The fault rocks such as breccia, fault gouge, pseudotachylite, or cataclasite are more challenging due to the nature of soil particles and rock block mixture, which exhibits strong non-homogenous, discontinuity, anisotropy, and environmental sensitivity. The engineering activities, such as rock mass blast vibration [1, 2], excavation [3, 4], and fluid injection or production [5, 6], affect the geo-stress such that they can even sometime reactive dominant faults in the vicinity. The reactivation of the fault zone would lead to the formation of very fine-grained, cohesionless fault gouge, and fragmentation of weathered rock. Medley [7] coined a term of bimrock or bimsoils (block-in-matrix rock or soil) to describe rocks that are composed of geotechnically significant blocks within a bonded matrix of finer texture and put the fault rocks into the range of bimrock. Plenty of studies have been performed to investigate the mechanical behavior of fault rocks and the associated fault reactivation induced by rock engineering construction. Krantz [8] conducted laboratory shearing test to measure the friction coefficient and cohesion of faulting and fault reactivation; the fault bimrock was prepared as a mixture of quartz sand, clay, and cement. They found a consistent drop in cohesion for fault reactivation in the dense mixtures. Mercuri et al. [9] conducted shear testing on fault gouges to reveal the brittle fault reactivation, and the strength weaken of the fault gouges was revealed from microstructural analysis. Giorgetti et al. [10] conducted triaxial experiments on fault rocks to investigate the reactivation of gouge-bearing faults, and the fault band is prepared on sandstone cylinders containing saw-cut filled with clay-rich gouge. By comparing their experiments to analytical models, they pointed out that the analytical model assumes a zero-thickness planar, this method provides an upper bound to fault reactivation, and the result may mislead

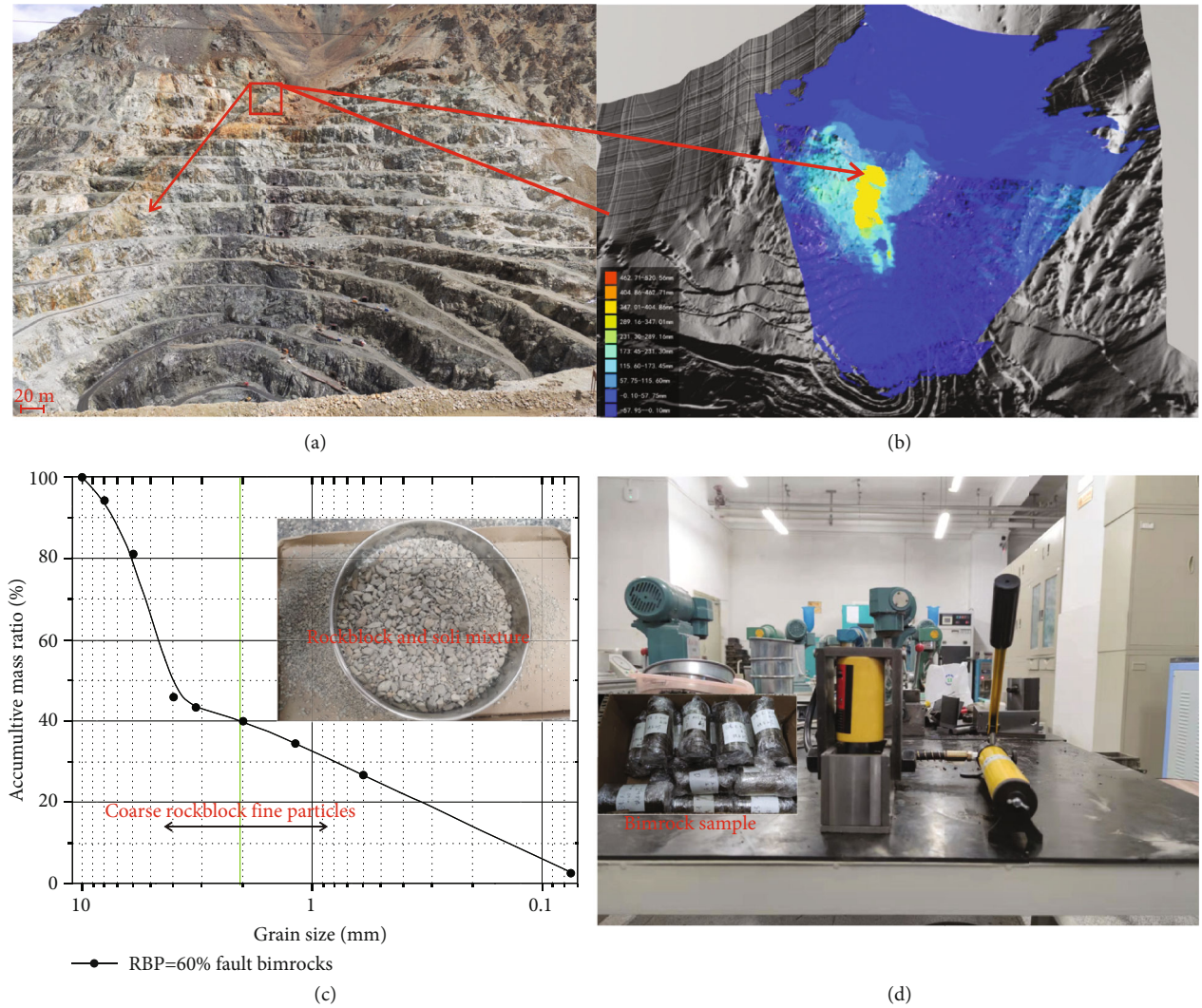

Figure 1: Description of fault bimrocks and fault reactivation in the Beizhan iron mine ((a) position of a normal fault on rock mass outcrop; (b) deformation detection by a synthetic aperture radar; (c) particle size distribution of rock blocks and soil matrix; (d) consolidation method to prepare bimrock samples).

the predication of fault reactivation. Brantut et al. [11] investigate creep test on clay-bearing fault gouge to reveal the high-velocity frictional properties. Ferri et al. [12] conducted experiments on smectite-rich gouge to study the high-velocity friction behaviors under thermal pressurization conditions. Sulem et al. [13] performed numerical studies on clay-bearing fault gouge to investigate the rapid shear characteristics. Yund et al. [14] used amorphous material to mimic artificial fault gouge and conducted high strain experiment; they found cyclic deformation allows the gauge to accommodate the passage of geometric irregularities on the active slip surfaces.

For the fault in cold regions, the frost heaving force forms within the rock-soil interfaces, pores, and microcracks, resulting in the damage propagation and increase of crack aperture and length, and deteriorating the bimrock structure. In addition, stress disturbance is inevitable during rock mass construction in the civil or mining engineering [15–18], and stress disturbance accelerates the reactivation of fault bimrock. Although plenty of studies have been performed about the freeze-thaw damage and stress disturbance on material fracture and instability, all most all of the investigations are focused on rock or soil material [19–23]. The geomechnical behaviors of bimrock subjected to freeze-thaw and stress disturbance is poorly understood. However, the fault reactivation in cold region is crucial to the mine stability, especially for the open-pit mining engineering, tunnel or roadway engineering, etc., and revealing the mechanical behaviors of fault bimrock is extremely urgent.

The basic purpose of this work is to reveal the effect of F-T and increasing-amplitude cyclic loads on damage and fracture evolution of a fault bimrock. An introduction section dealing with literature review has been included in the first section. In section two, experimental methodology was explained particularly about the preparation of bimrock samples and testing procedures. In section three, the coupled damage evolution caused by the freeze-thaw cycle and cyclic loads on bimrock was deeply investigated. This work is

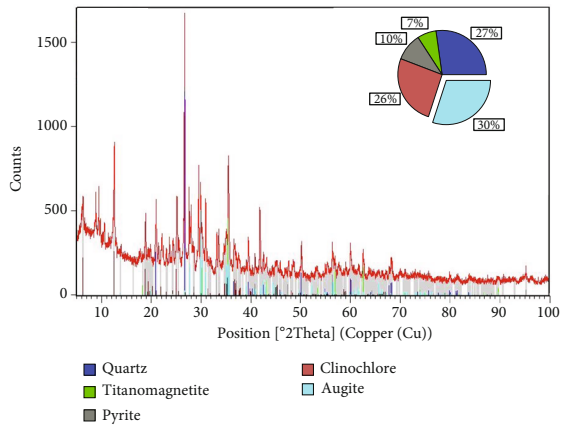

(a)

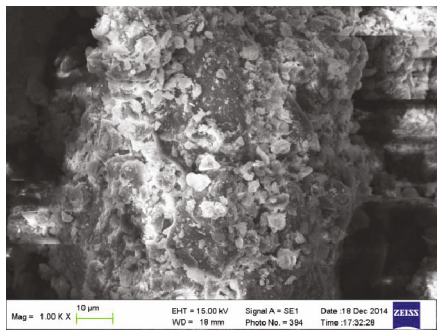

(b)

Figure 2: Mesoscopic structure description of the soil matrix ((a) XRD result; (b) SEM result).

emphatically focused on the effect of F-T and stress disturbance on bimrock mechanical response and the associated fault reactivation.

2. Methods

2.1. Preparation of Bimrock Sample. The bimrock material is composed of the soil matrix and rock blocks, and these two kinds of materials were obtained from the outcrop fault in the Hejing Beizhan iron mine in the Xinjiang province, northwest of China, see Figure 1(a). The fault starts to reactivation during hang-wall ore exploitation, and the impact of fault reactivation on slope deformation is monitored by a synthetic aperture radar, see Figure 1(b). At an altitude of 3360 m ~3655 m, it can be seen that fault instability sliding occurs due to the mining activities and repeated freeze-thaw cycles. Therefore, study the mechanical behaviors of fault bimrock subjected to freeze-thaw and stress disturbance is critical to the mine safety.

The bimrock sample is the mixture of soil particles and rock blocks, and the sieve test result reveals the grain composition characteristics, as shown in Figure 1(c). The proportion of rock blocks is about 60%, and this result reveals a high rock block percentage for the studied bimrock. XRD result in Figure 2(a) indicates the mineral composition of the soil matrix; it is found that the matrix is mainly composed of quartz, titanomagnetite, pyrite, cinochlore, and augite; and their proportion is 27%, 7%, 10%, 26%, and 30%, respectively. SEM result in Figure 2(b) reveals the mesoscopic structure of rock matrix, it has inhomgeneous structure, and several microcracks and mineral interfaces were observed. In addition, a large number of microcracks are distributed around the minerals. The basic physical and mechanical parameters of the soil matrix and rock blocks are listed in Table 1.

Table 1: Description of the bimrock samples under freeze-thaw-fatigue loads.

Sample ID	$L \times d$ (mm × mm)	F-T cycle	Mass (g)	Density (g/cm^3)	P-wave velocity (m/s)
BIM-0-1	99.87 × 49.23	0	475.12	2.602	1520
BIM-0-2	99.77 × 50.01	0	469.65	2.519	1590
BIM-0-3	99.56 × 49.76	0	447.23	2.501	1550
BIM-0-4	99.86 × 49.55	0	480.08	2.451	1580
BIM-20-1	99.82 × 49.66	20	473.68	2.513	1410
BIM-20-2	99.80 × 50.02	20	473.66	2.515	1430
BIM-20-3	99.67 × 49.67	20	470.96	2.504	1434
BIM-20-4	99.88 × 49.45	20	485.02	2.522	1472
BIM-40-1	99.59 × 50.01	40	482.22	2.501	1300
BIM-40-2	99.45 × 50.02	40	479.26	2.509	1295
BIM-40-3	99.76 × 49.88	40	478.06	2.469	1320
BIM-40-4	99.55 × 49.67	40	475.22	2.495	1356
BIM-60-1	99.80 × 50.02	60	471.11	2.403	1026
BIM-60-2	99.67 × 49.67	60	459.32	2.511	1001
BIM-60-3	99.88 × 49.45	60	467.26	2.493	1020
BIM-60-4	99.59 × 50.01	60	485.22	2.395	1050

The bimrock samples were remolded in the laboratory, and a consolidation sample preparation method is used to produce bimrock sample with a diameter of 50 mm and height of 100 mm. The sample device is specially designed to prepared remolded samples; it is mainly composed of iron mould, jack, hand pump, and pressure gauge and displacement meter. First, the soil and rock blocks were mixed, a 20% water was added in the mixture, manual mixing sample preparation is adopted, and the mixture was sealed with 24 hour; second, the required mixture to prepared one bimrock sample was taken and put into the iron mould. After the specimen is pressed to a fixed size, it is continued to be

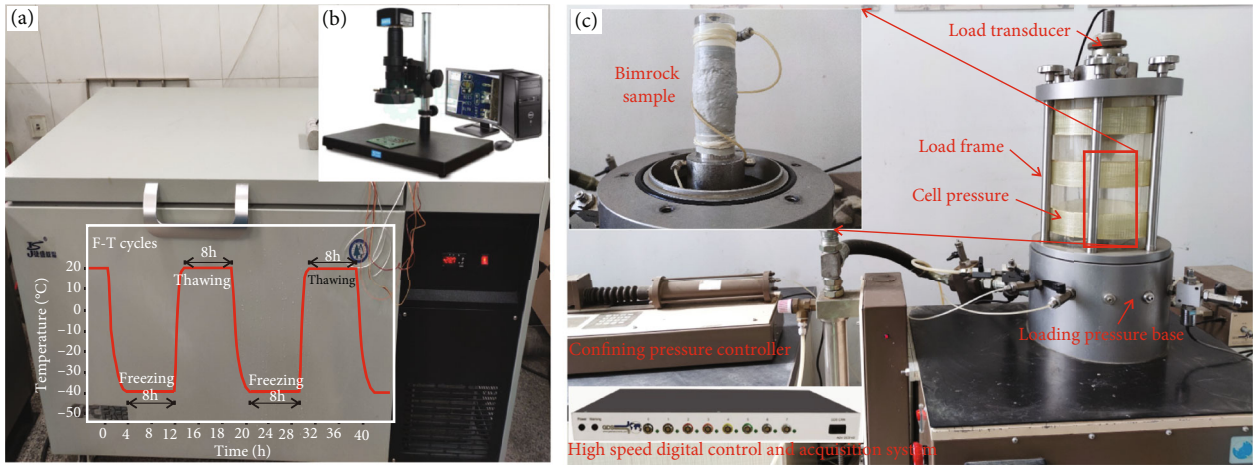

Figure 3: The testing apparatus in the freeze-thaw-fatigue experiment for the bimrock sample ((a) the ultralow environmental box; (b) electron microscope; (c) GDS DYNTTS testing apparatus).

loaded with a jack and consolidated for 1 h. Finally, the consolidated sample was taken out of the mould. A total of 16 bimrock samples were prepared, and four groups were divided to perform FT tests with FT cycle of 0, 20, 40, and 60, respectively. Every two typical samples with the same FT treatment were used to conduct fatigue mechanical tests.

2.2. Testing Equipment. The prepared bimrock samples were subjected to different FT cycles in an ultralow temperature environmental box (Figure 3(a)). After each FT cycle, electron microscope (Figure 3(b)) was employed to observe the mesoscopic structure change of the soil-block interface and the soil matrix. Afterward, multistage increasing-amplitude cyclic loading testing was carried out on the bimrock sample using a GDS DYNTTS system, see Figure 3(c). The GDS DYNTTS testing system is capable of very small strain static tests through to large strain dynamic tests. It is equipped with a kind of high accuracy electromechanical device, and the axial force accuracy is less than 0.1%. The maximum dynamic frequency is 5 Hz, the maximum axial load is 60 kN, and it is capable of the direct closed loop of axial displacement and axial force. The axial load resolution is less than 1.5 N, and displacement resolution is less than 0.2 μm. During cyclic loading experiment, the bimrock axial strain and axial stress can be collected at the same sampling frequency. In this work, the consolidated drained (CD) triaxial cyclic loading tests were performed, and the volumetric strain is obtained from the output water volume.

2.3. Testing Procedures. The prepared bimrock samples were subjected to freeze-thaw treatment and multistage increasing-amplitude cyclic loads, and the loading scheme is listed in Table 2. A detailed description of the testing procedures is summarized as below:

(1) *Freeze-Thaw Treatment.* The upper and lower temperatures for FT testing were chosen according to the actual temperature variations at the Beizhan open pit over the course of a year. An 8 h freezing period (−40°C) and an 8 h thawing period (+20° C) were applied to bimrock to simulate FT cycles of the rock in the mine. In addition, 8 hours are long enough to reach a completely frozen state or thawed state. In the laboratory, the hydrous sample was frozen in the F-T machine at −40°C for 8 h; then, the sample was taken out of the ultralow environmental box and thawed in the air, and this is a complete F-T cycle. After each FT cycle, the ultrasonic pulse velocity was measured. The FT cycle for the tested rock is set to be 0, 20, 40, and 60, respectively

(2) *Multistage Cyclic Loading Test.* First, the sample was loaded to a stress of 100 kPa at a constant deformation rate of 0.2 mm/min. Following the static loading path, the sinusoidal cyclic loads controlled by stress is applied, and the stress amplitude is 100 kPa at the first cyclic loading stage (CLS). In each subsequent cyclic loading stage, the stress amplitude increased by 100 kPa until sample failure. The cyclic load is programmed in advance and realized by the computer, the loading frequency is 0.5 Hz, that is, a cycle with a loading and unloading duration can be completed within 2 seconds. In each CLS, a total of 100 stress cycles were applied to the bimrock samples. The loading scheme is shown in Figure 4

(3) After the mechanical tests, the macroscopic failure morphology was observed to reveal the interactions between rock blocks and soil matrix

3. Results and Analyses

3.1. Cyclic Stress Strain Curves. The typical fatigue stress-strain curves for the freeze-thawed bimrock samples are plotted in Figure 5. During the sample preparation, all the samples are prepared to have the same rock block percentage and block distribution as possible. It is shown in Figure 5 that the previous freeze-thaw damage influences the fatigue strength, fatigue deformation, and lifetime of bimrock. Under the same loading paths, the CLS is 6, 5, 5, and 4, respectively, for bimrock subjected to FT cycle of 0, 20, 40, and 60. The corresponding

Table 2: The testing schemes for the multilevel cyclic loading tests.

Sample ID	FT cycle (cycle)	σ_{min} (kPa)	σ_{max}^{i} (kPa)	σ_a (kPa)	σ_{max}^{f} (kPa)	CLS (/)	Cycle of each CLS (cycle)	f (Hz)
BIM-0-1,2	0	100	100	100	700	6	100	0.5
BIM-20-1,2	20	100	100	100	500	4	100	0.5
BIM-40-1,2	40	100	100	100	500	4	100	0.5
BIM-60-1,2	60	100	100	100	400	3	100	0.5

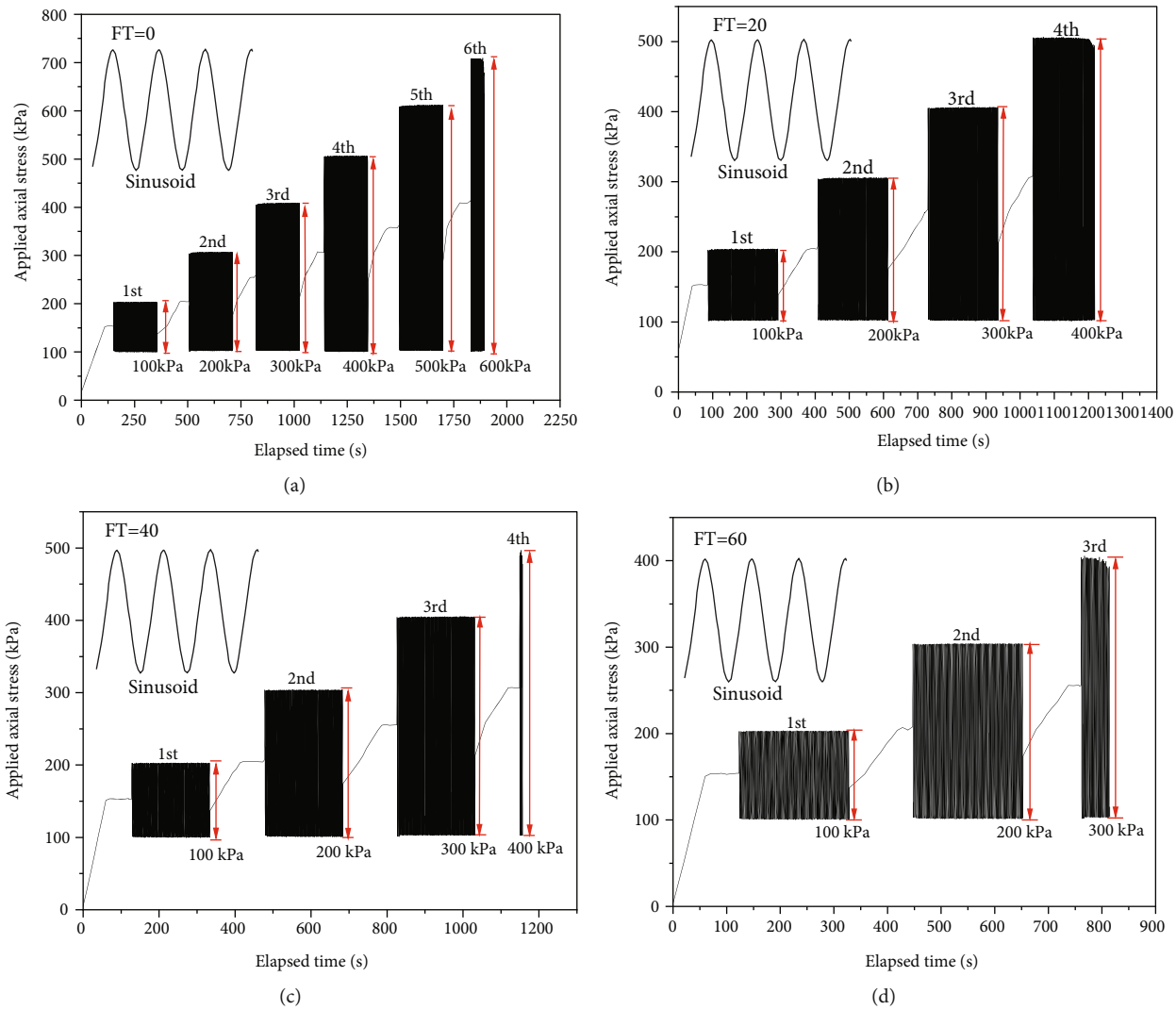

Figure 4: The loading paths of the tested granite containing two fissures and a hole ((a)–(d) rock samples experience F-T cycle of 0, 30, 60, and 90, respectively).

fatigue lifetime is 553, 491, 423, and 227, respectively. Impacted by the previous FT treatment, the differential damage at the soil-rock interfaces leads to the different performance to resist external loads, and the fatigue strength decreases with the increase of FT cycle. The fatigue mechanical parameters are summarized in Table 3.

From the stress-strain curves, it is also shown that the loading curve is not overlapped with the unloading curve and stress hysteresis loop during deformation. The hysteresis loop presents a first sparse and then dense pattern at the first several CLS, however, it becomes more and more sparse at the final CLS and exhibiting a sparse-dense-sparse pattern. The sparse pattern at the onset of a CLS implies the generation of relatively large damage caused by the increase of stress amplitude and the damage increases steadily with increasing loading cycle at a CLS. At the final CLS, the previous accumulative damage accelerates rock failure, and the interval and area of hysteresis loop become larger and larger. The number

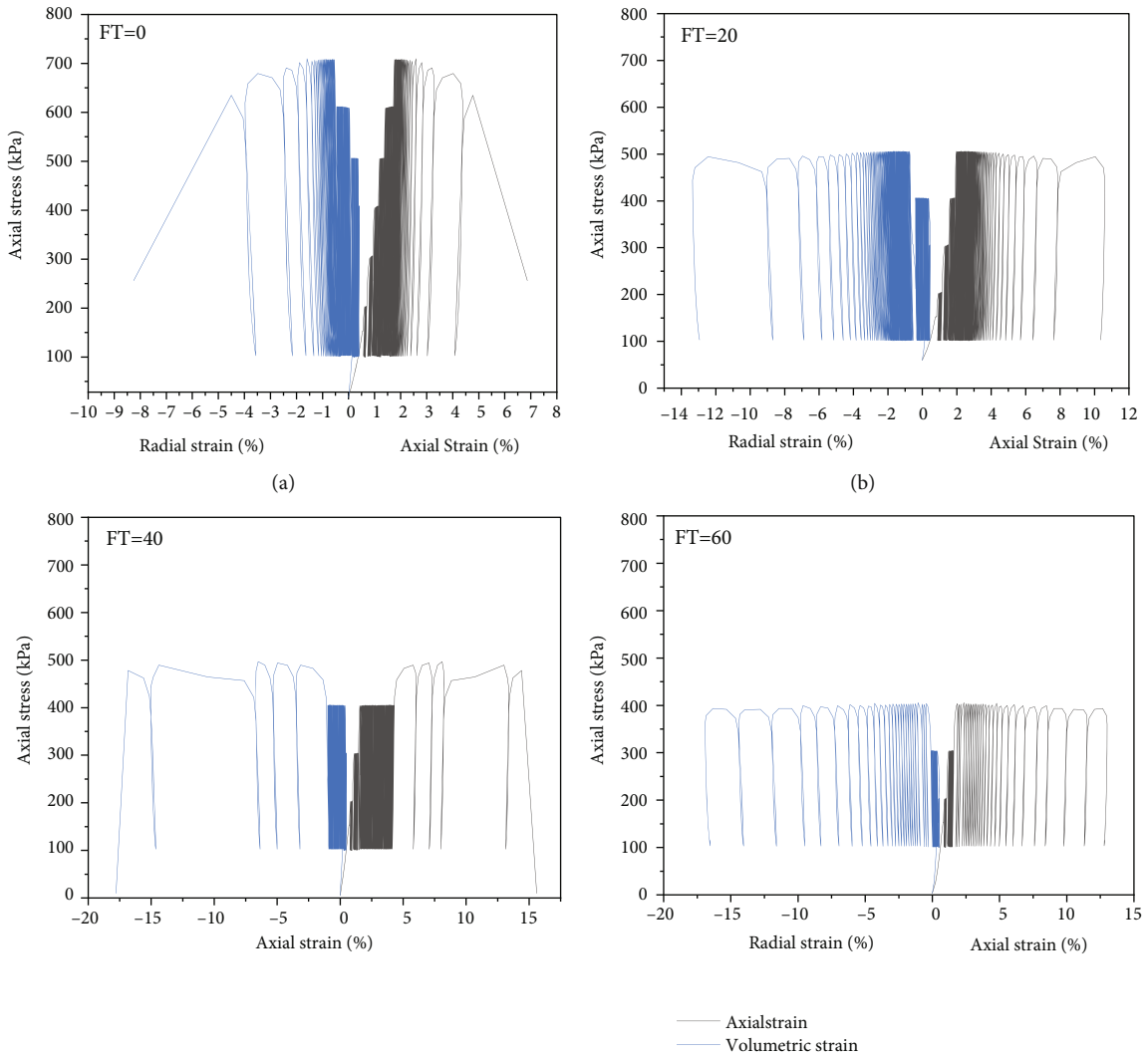

Figure 5: Typical stress-strain responses of the bimrock samples under multistage cyclic loads ((a)–(d) bimrock samples experience F-T cycle of 0, 20, 40, and 60, respectively).

Table 3: Summarization of the mechanical parameters of the tested bimrock samples.

Sample ID	$L \times d$ (mm × mm)	F-T cycle	Peak axial stress (kPa)	Peak axial strain (%)	Peak volumetric strain (%)	Loading stage	Loading cycles
BIM-0-1	100.01 × 49.39	0	700	6.786	-8.351	6	553
BIM-0-2	99.89 × 50.05	0	800	8.232	-9.032	6	625
BIM-20-1	99.62 × 49.95	20	500	10.602	-13.355	4	491
BIM-20-2	99.62 × 49.95	20	600	11.368	-12.665	5	522
BIM-40-1	99.89 × 50.05	40	500	13.388	-15.042	4	423
BIM-40-2	99.62 × 49.95	40	500	12.031	-15.985	4	444
BIM-60-1	99.89 × 50.05	60	400	13.007	-16.913	3	227
BIM-60-2	99.62 × 49.95	60	400	16.765	-18.002	3	256

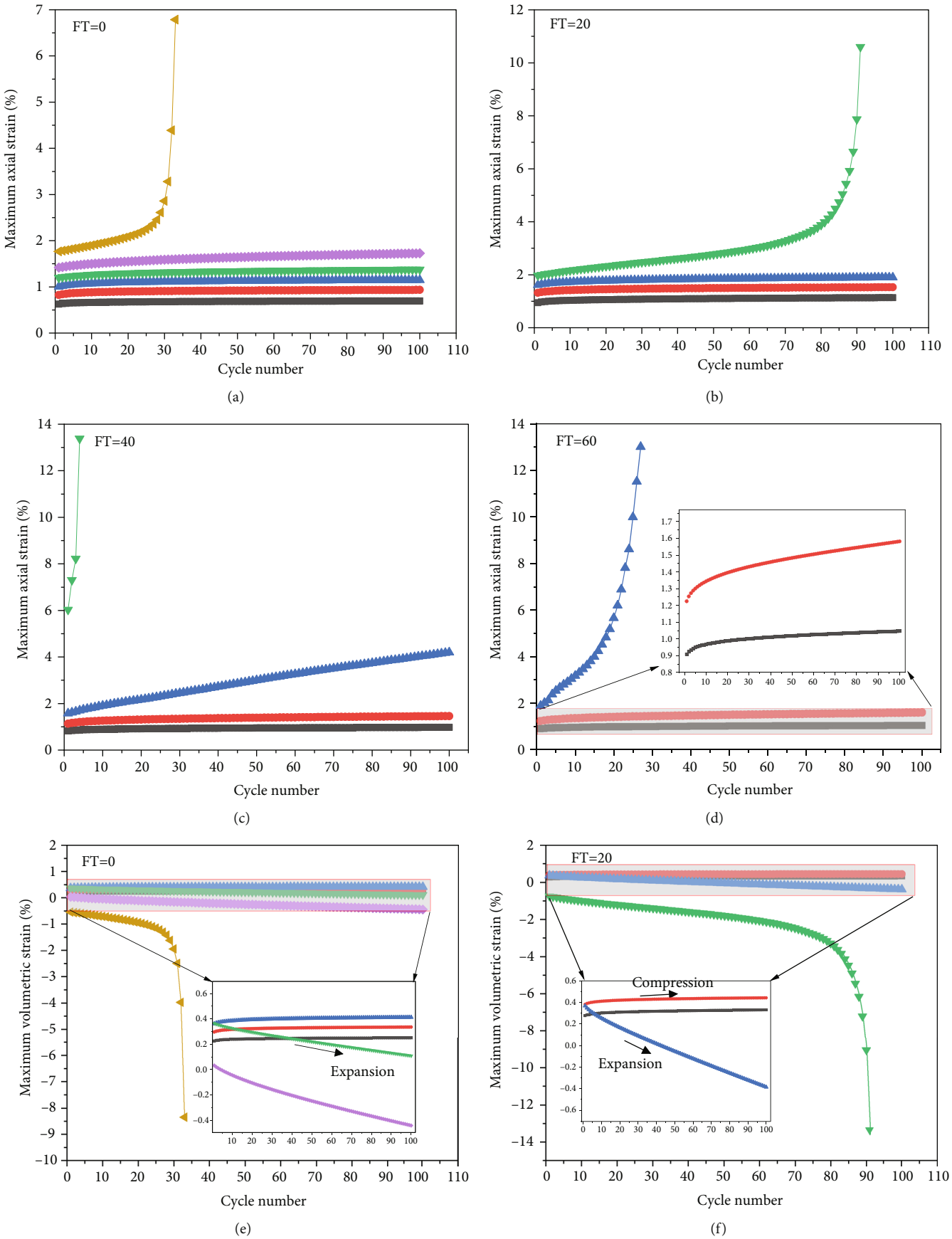

Figure 6: Continued.

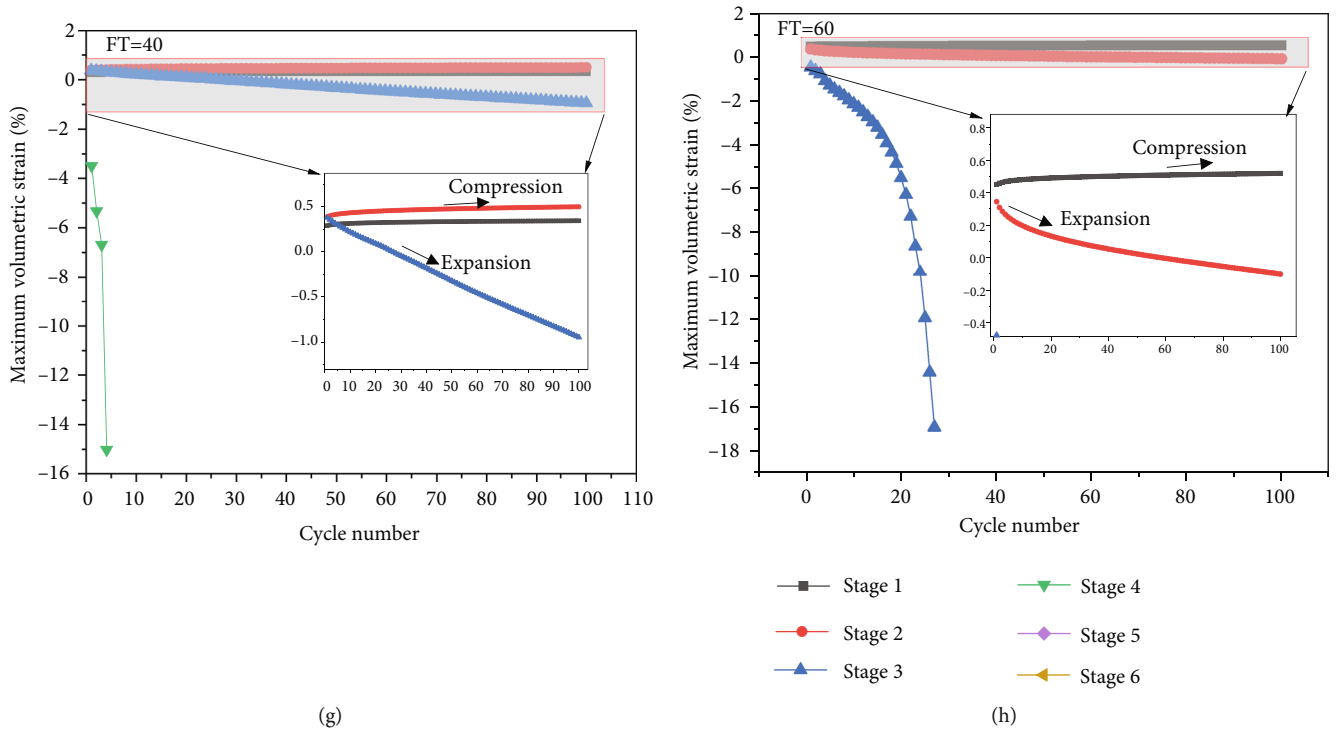

(g) (h)

Figure 6: Fatigue deformation characteristics of the freeze-thawed bimrock samples ((a)–(d) axial strain versus cycle number at different CLS; (e)–(h) the volumetric strain versus cycle number at different CLS).

of the hysteresis loop at the last cyclic loading stage is 53, 91, 23, and 27, respectively. Because the rock block percentage of the fault bimrock is high, i.e., 60% in this work, the interlocking and occlusion degrees among the rock blocks are high, and the bimrock sample failures progressively and not a sudden stress drop.

3.2. Bimrock Deformation Characterization. The formation of stress hysteresis loop indicates the occurrence of plastic deformation during fatigue loads. Figure 6 presents the axial, radial, and volumetric deformation during the entire loading process. The axial strain is measured by a displacement transducer at the GDS testing system, see Figures 6(a)–6(d). It is observed in Figures 6(a)–6(d) that the axial strain within a CLS is relatively small before the finial loading stage; however, the increasing rate of axial strain between each cyclic stage increases sharply. The accumulative damage at the previous cyclic loading stage has obvious impact on rock axial deformation. Within a CLS, the axial strain shows a quick increase then steady increase trend except the last CLS. The first quick increase of axial strain indicates that the damage is relatively large at the increasing-amplitude moment; then, the damage propagates steadily. However, at the last CLS, the axial strain increases sharply until sample failure. Owing to water-ice phase transformation and the generation of frost heaving force in bimrock (e.g., interfaces, pores, and microcracks), bimrock is encountered with mesoscopic structural degradation, and inhomogeneous deformation occurs under cyclic loads. It is shown that the incremental pattern of the axial strain is different, and it is shown that increase of axial strain is relatively quick for rock subjected to high FT cycle. Especially, at the last CLS, the growth rate of the axial strain is quicker for rock subjected to 40 and 60 FT cycles.

Because the consolidated-drained cyclic loading tests are performed for the bimrock samples, the radial strain can be obtained by the ratio of mean diameter variation to the original sample diameter. As a result, the volumetric strain (εv) calculated as $\varepsilon_v = \varepsilon_1 + 2\varepsilon_3$, where ε_1 is the axial strain and ε_3 is the radial strain. The relationship between the maximum volumetric strain and cycle number is plotted in Figures 6(e) and 6(f). The change of the volumetric strain in Figures 6(e) and 6(f) shows that bimrock sample experiences first compression-dominant and then expansion-dominant process. The previous FT treatment influences rock volumetric change, and the inflection CLS is 4^{th}, 3^{rd}, 3^{rd}, and 2^{nd}. The damage deterioration of rock-soil interfaces influences the initiation, propagation, and coalescence of the cracks; and this results in the difference of failure morphology. The dilatancy effect is much more obvious for bimrock subjected to 40 and 60 FT than those of 0 and 20 FT cycles. The final volumetric strain is -8.351%, -12.665%, -15.042%, and -18.002%, respectively, for bimrock exposed to 0, 20, 40, and 60 FT cycles.

3.3. Stiffness Changes during Bimrock Deformation. For the tested bimrock samples, the stiffness change is characterized by a defined index of secant modulus (Es). Es is the line slope that joints the below limit stress and the upper limit stress of each cycle in the axial stress-strain curves. The change of Es is plotted in Figure 7. It is shown that Es decreases in a CLS, and it decreases quickly at the first several cycles and then it gets to steady. The steady of Es within a CLS indicates that the coupling degree among the rock blocks and soil matrix improves

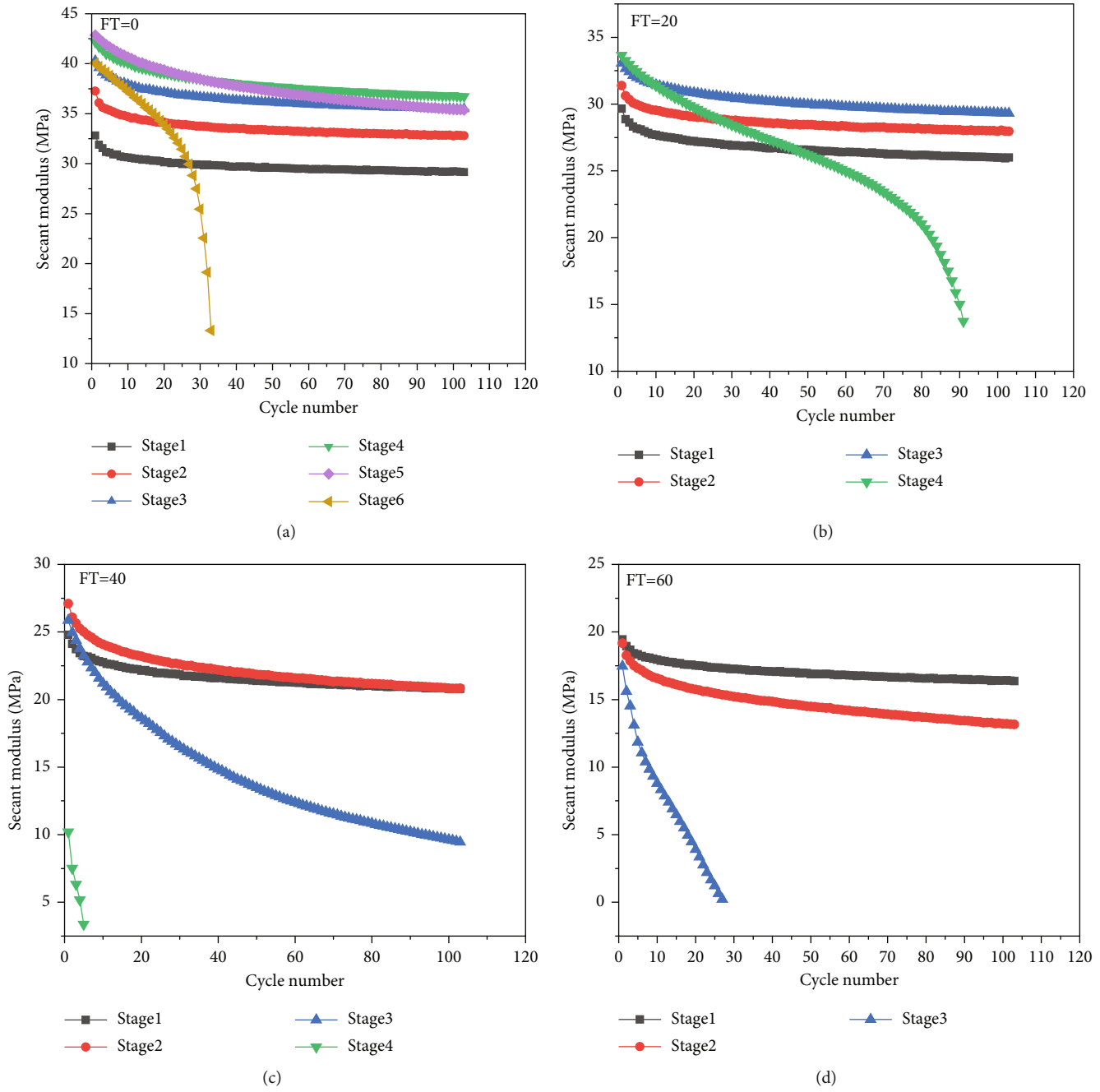

Figure 7: Depict of secant modulus with cycle number during bimrock deformation ((a)–(d) the tested sample experience 0, 20, 40, and 60 FT cycles).

accordingly. We can also see that the Es presents a decrease trend as FT cycle numbers. It is the largest for rock subjected to 0 FT cycle and smallest for rock subjected to 60 FT cycle. For a tested bimrock samples, Es presents a first increase and then decrease trend. The increase of Es reflects the compaction of soil matrix and the improvement of coupling degree among the rock matrix and rock blocks. After several CLS, Es starts to decrease due to the cracking in the rock-soil interface and the movement of rock blocks in bimrock. The onset of decreasing CLS is 5^{th}, 4^{th}, 3^{rd}, and 2^{nd}, respectively.

3.4. Coupled Damage Characteristics Subjected to F-T-Fatigue Loads. For the freeze-thawed bimrock samples in this work, they are subjected to two kinds of fatigue damage, one is induced by the previous freeze-thaw treatment, and the other is the mechanical loads. As a result, the coupling damage of the freeze-thaw and mechanical loads was considered simultaneously herein. Owing to the differential freeze-thaw actions on bimrock samples, the increase of porosity in soil matrix and cracking of rock-soil interface both lead to the entire structural deterioration of bimrock. To reveal the

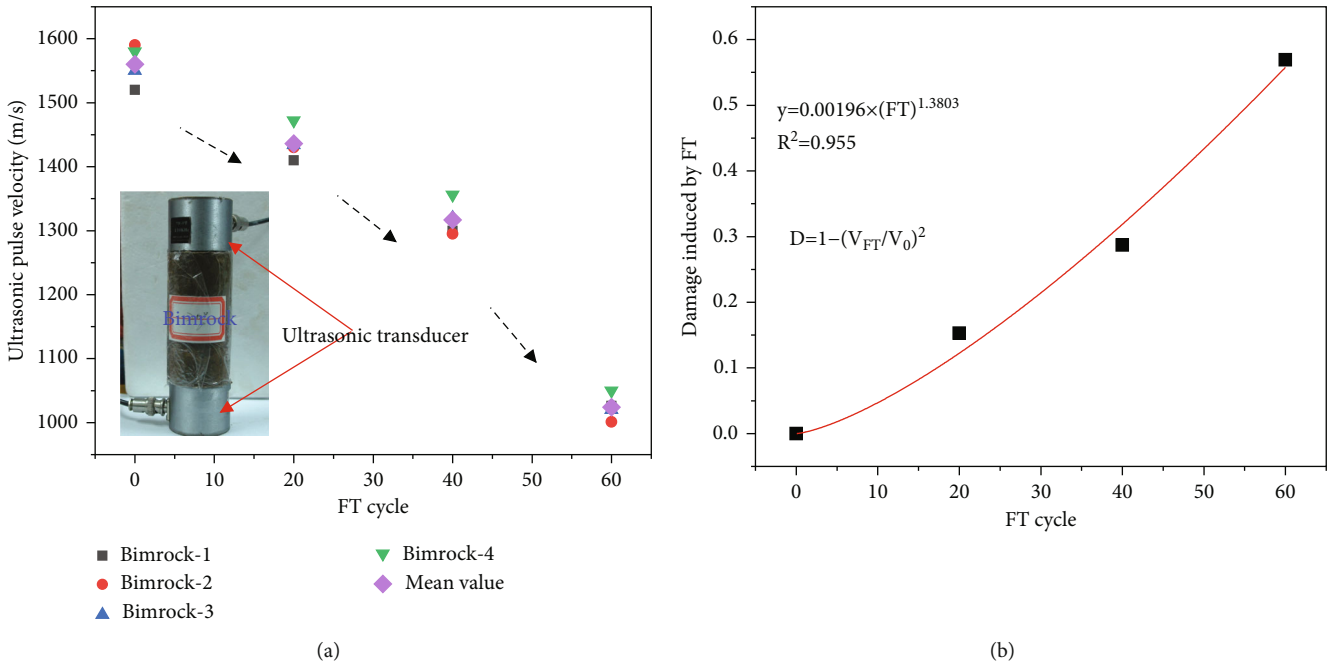

FIGURE 8: Structural deterioration of the bimrocks described by the ultrasonic velocity ((a) the ultrasonic velocity versus FT cycle; (b) FT induced damage versus FT cycle).

entire damage characteristics resulting from the FT treatment, ultrasonic measurement is employed to obtain the velocity for the bimrock subjected to different FT cycles, see Figure 8(a). The velocity decreases with the increase of FT cycle, and the reduce rate becomes fast. The damage caused by the previous FT treatment is quantitatively characterized by a damage factor defined by velocity, as shown in Figure 8(b). It is shown that there exists a power relationship between the damage factor and FT number. It can be observed that the damage degree of the freeze-thawed bimrock increases with the increase of F-T cycle, and the increasing rate becomes faster and faster. The equation fitting is used to establish the link between the F-T damage and F-T cycle, it is found that a power function can well describe the changing trend of F-T induced damage, and it is shown as

$$D_{F-T} = 0.00196 \times (\mathrm{FT})^{1.3803} \mathrm{Adj}.R^2 = 0.955, \quad (1)$$

where D_{F-T} refers to the damage induced by the previous F-T treatment, and N represents the F-T cycle. It stands for the number of F-T cycles. The Adj.R^2 is a modification of R^2 that adjusts for the number of explanatory terms in a model when taking the sample size into consideration.

For bimrock subjected to increasing-amplitude cyclic loads, the effect of the previous freeze-thaw damage on rock accumulative damage at each cyclic loading stage is displayed in Figure 8(b). It can be seen that F-T inducted damage degree increases with increasing F-T cycles. At the same cyclic loading stage, F-T inducted damage is relatively high for a rock subjected to high F-T treatment. Under the fatigue loads, as the axial strain can be precisely obtained from the displacement transducer, a damage variable defined using the axial strain is employed to reflect the mechanical damage induced by cyclic loads. In addition, the previous studies have proved the reliability to use axial strain to express rock damage evolution [23–25]. Therefore, the damage index defined by axial strain is introduced herein, as shown as follows:

$$D_f = \frac{\varepsilon_d}{\varepsilon} \frac{\varepsilon - \varepsilon_0}{\varepsilon_d - \varepsilon_0}, \quad (2)$$

where D_f is the damage factor caused by fatigue loads, ε_d is the axial strain at the failure point, ε_0 is the axial strain at the first CLS and the first cycle, ε is the strain during rock deformation, and ε_d is the axial strain and the failure point. Based on Eq. (2), the damage variable for rock at each loading cycle is shown in Figure 9. It is found that a two-stage damage evolution pattern exits for the bimrock sample at different CLS except the final CLS, and the damage increases faster and then gets to steady with a CLS. At the last CLS, three-stage damage evolution characterized with a first fast followed by a steady growth and then quick growth occurs for all the tested bimrock samples. In addition, it is found that damage increases with increasing FT cycle at the same CLS.

As stated above, for the fault bimrock sample subjected to freeze-thaw and cyclic loads, damage includes two parts, one is the previous freeze-thaw fatigue damage, and the other part is the mechanical loads. The damage induced by freeze-thaw and increasing-amplitude cyclic loads is calculated from Eq. (1) and (2). Therefore, the coupling damage is obtained as

$$D_{\mathrm{coupling}} = D_{F-T} + D_f - D_{F-T} \times D_f. \quad (3)$$

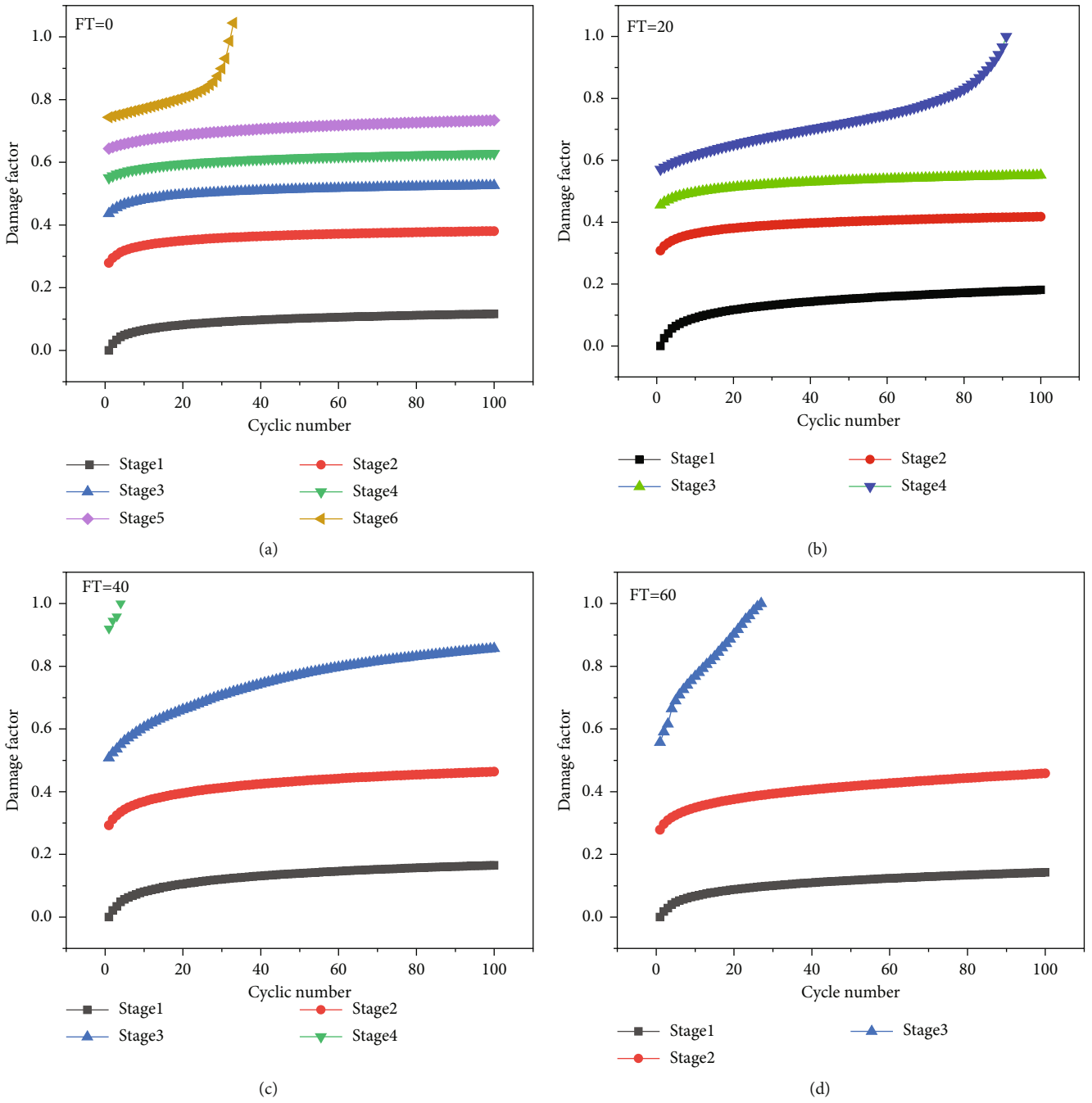

Figure 9: Damage evolution for bimrock at different CLS ((a)–(d) bimrock sample subjected to of 0, 20, 40, and 60 FT cycles, respectively).

After obtaining the coupling damage variable, the relationship between the coupling damage variable and relative cycle is presented in Figure 10. Considering the effect of the previous freeze-thaw damage, the coupling damage is larger than the mechanical damage, and the evolution curve of the accumulative damage displays different patterns for the rock samples subjected to 0, 20, 40, and 60 F-T cycle. The damage trend in Figure 10 shows two-stage and three-stage damage for the tested bimrock samples. For bimrock sample without FT treatment, damage propagates relatively slow, damage begins to occur only when the applied loading reaches a certain value, and this is the typical two-stage damage evolution pattern. However, for rock subjected to high FT cycles, rock-soil interface damages and cracks before the mechanical loads. When subjecting to the cyclic loads, damage propagates quickly at the initial loading stages; then, rock was compacted and damage propagates steady; at high cyclic loading level, damage propagates rapidly until rock failure. This progress is the typical three-stage damage evolution pattern.

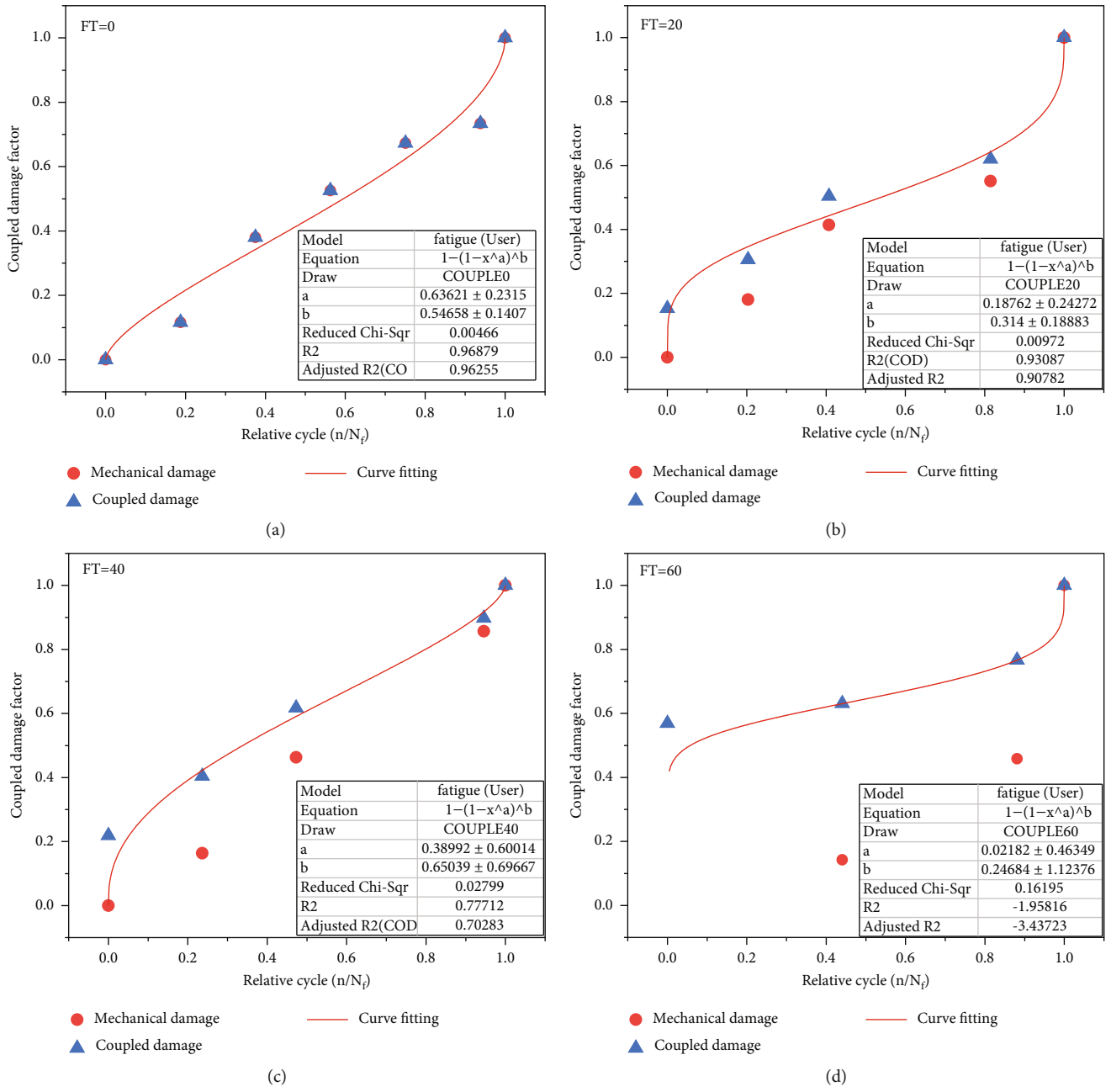

Figure 10: Curve fitting of the accumulative damage at the end of each cyclic loading level ((a)–(d) the rock samples experience F-T cycle of 0, 30, 60, and 90, respectively).

Table 4: Fitting relationship between the coupling damage and relative cycle.

F-T cycle	$D_{coupling} = 1 - (1 - (n/N_f)^a)^b$		R^2
	a	b	
0	0.636	0.546	0.915
20	0.187	0.315	0.907
40	0.389	0.651	0.778
60	0.022	0.249	0.855

According to the two-stage and three-stage damage accumulation pattern in Figures 10(a)–10(d), a new damage evolution model is proposed and its form is shown as

$$D_{coupling} = 1 - \left(1 - \left(\frac{n}{N_f}\right)^a\right)^b, \quad (4)$$

where D is the damage variable caused by the irreversible plastic deformation, the rock damage is 0 before loading ($N = 0$), and it is 1 ($N = N_f$) when it fails completely; n is the number of loading cycles; N_f is the fatigue life; a and b are related to

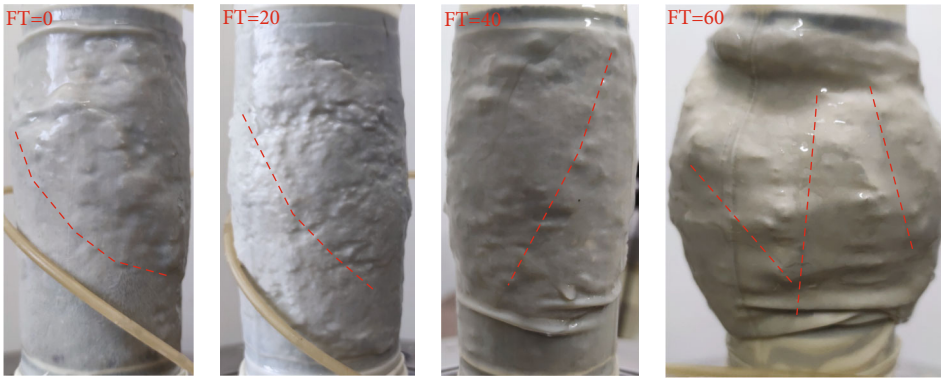

Figure 11: Macroscopic failure morphology of the freeze-thawed bimrock samples.

the material parameters. The fitting result for rock experiencing 0, 20, 40, and 60 FT cycle is shown in Figure 10. Good correlation was found between the damage variable and relative cycle. The fitting equations have high correlation coefficients of 0.915, 0.907, 0.778, and 0.855, respectively, as listed in Table 4.

3.5. Failure Morphology Analysis. The failure mechanism of bimrock subjected to cyclic loads can be analyzed form the macroscopic failure morphology, see Figure 11. Under uniaxial cyclic loads, the failure pattern is obviously impacted by the previous freeze-thaw treatment, and it can be seen that the volumetric expansion of bimrock is the largest for a sample subjected to 60 FT cycles. The dip angle of the main failure plane is not smooth, and its shape is impacted by the existence of rock blocks. The cracks propagate and negotiate the rock blocks, and multiple cracking segments communicate leading to the formation of the macroscopic failure surface. The morphology of the failure surface is totally different from the soil and rock material [26, 27], and the failure morphology is also different from bimrock under conversional uniaxial compression [28–30]. For sample subjected to 0, 20, and 40 FT cycles, shear failure occurs, however, bulging failure occurs for a sample subjected to 60 FT cycles. The differential failure morphology indicates that bimrock is sensitive to FT cycles, this is to say, the soil-rock interface is easily be deteriorated under FT conditions. As the tested bimrock samples have relatively high rock block percentage under cyclic loads, the interlocking, occlusion, contact, and separation occur frequently. The existence of bimrock blocks the propagation of cracks, and instability is obviously influenced by the block position, size, and distribution.

4. Conclusions

In this paper, freeze-thaw-fatigue tests were performed on bimrock samples; the influences of the freeze-thaw on the structural deterioration, strength, deformation, and damage evolution were systematically investigated. According to the analysis above, some key conclusions are drawn below:

(1) Due to the high elasticity mismatch between the fine-grained soil particles and coarse rock blocks, the soil-interface is sensitive to freeze-thaw condition. Interface damage and cracking contributes a lot to sample strength, volumetric deformation, and damage evolution

(2) Damage development for bimrock under cyclic loads usually shows a two-stage mode, and the sudden increase of stress amplitude results in the sharp damage of bimrock. Afterward, the coupling degree bimrock improves with the increase of loading cycles

(3) A coupling freeze-thawed and mechanical damage evolution model was proposed using the damage index defined by ultrasonic velocity and axial strain. The model fits well to the two-stage and three-stage damage accumulation. The model fits well with the testing date, and it is suggested that damage propagation is faster for rock subjected to high FT treatment. It is found that the evolution trend of the model is strongly related to the previous freeze-thaw damage

(4) Failure morphology of the bimrocks is strongly impacted by the freeze-thaw cycles, especially the existence of soil-block interfaces accelerate the structural deterioration of bimrock. Failure mode changes from shear failure to bulging failure. The failure process of bimrock is the rearrangement of the fine soil particles and rock blocks, the soil matrix, and rock block bear axial cyclic loads by their interactions

Data Availability

The experimental data used to support the findings of this study are included within the article.

Conflicts of Interest

The authors declare no conflict of interest.

Authors' Contributions

Yu Wang did the supervision, funding acquisition, and project administration; Hongjian Wang did the experiments

and data analysis; Tao Sun did the methodology and conceptualization; Xuefeng Yi did the visualization, data curation, and resources.

Acknowledgments

This study was supported by Beijing Natural Science Foundation (8202033), Key Laboratory of Geological Environment Intelligent Monitoring and Disaster Prevention and Control of Henan Province, North China University of Water Resources and Electric Power (ZDZX2020001), National Natural Science Foundation of China (52174069), National Key Technologies Research & Development Program (2018YFC0808402), and the Fundamental Research Funds for the Central Universities (FRF-TP-20-004A2).

References

[1] M. R. Islam and R. Shinjo, "Mining-induced fault reactivation associated with the main conveyor belt roadway and safety of the Barapukuria coal mine in Bangladesh: constraints from BEM simulations," *International Journal of Coal Geology*, vol. 79, no. 4, pp. 115–130, 2009.

[2] Y. Wang, W. K. Feng, R. L. Hu, and C. H. Li, "Fracture evolution and energy characteristics during marble failure under triaxial fatigue cyclic and confining pressure unloading (FC-CPU) conditions," *Rock Mechanics and Rock Engineering*, vol. 54, no. 2, pp. 799–818, 2021.

[3] H. Xing and Z. Han, "Caving-induced fault reactivation behaviour and its effects on mining safety with a multiple seam context," *Acta Geotechnica*, vol. 15, no. 12, pp. 3461–3481, 2020.

[4] Y. Wang, C. Zhu, Z. Y. Song, and S. Gong, "Macro-meso failure characteristics of circular cavity-contained granite under unconventional cyclic loads: a lab-scale testing," *Measurement*, vol. 188, p. 110608, 2022.

[5] M. Lesueur, T. Poulet, and M. Veveakis, "Three-scale multiphysics finite element framework (FE3) modelling fault reactivation," *Computer Methods in Applied Mechanics and Engineering*, vol. 365, p. 112988, 2020.

[6] H. Soltanzadeh and C. D. Hawkes, "Assessing fault reactivation tendency within and surrounding porous reservoirs during fluid production or injection," *International Journal of Rock Mechanics and Mining Sciences*, vol. 46, no. 1, pp. 1–7, 2009.

[7] E. W. Medley, *The Engineering Characterization of Melanges and Similar Block-in-Matrix Rocks (Bimrocks)*, Doctoral dissertation, University of California, Berkeley, 1994.

[8] R. W. Krantz, "Measurements of friction coefficients and cohesion for faulting and fault reactivation in laboratory models using sand and sand mixtures," *Tectonophysics*, vol. 188, no. 1-2, pp. 203–207, 1991.

[9] M. Mercuri, M. M. Scuderi, T. Tesei, E. Carminati, and C. Collettini, "Strength evolution of simulated carbonate-bearing faults: the role of normal stress and slip velocity," *Journal of Structural Geology*, vol. 109, pp. 1–9, 2018.

[10] C. Giorgetti, T. Tesei, M. M. Scuderi, and C. Collettini, "Experimental insights into fault reactivation in gouge-filled fault zones," *Journal of Geophysical Research: Solid Earth*, vol. 124, no. 4, pp. 4189–4204, 2019.

[11] N. Brantut, J. R. Schubnel, F. Brunet, and T. Shimamoto, "High-velocity frictional properties of a clay-bearing fault gouge and implications for earthquake mechanics," *Journal of Geophysical Research*, vol. 113, no. B10, article B10401, 2008.

[12] F. Ferri, G. DiToro, T. Hirose, and T. Shimamoto, "Evidence of thermal pressurization in high-velocity friction experiments on smectite-rich gouges," *Terra Nova*, vol. 22, no. 5, pp. 347–353, 2010.

[13] J. Sulem, P. Lazar, and I. Vardoulakis, "Thermo-poro-mechanical properties of clayey gouge and application to rapid fault shearing," *International Journal for Numerical and Analytical Methods in Geomechanics*, vol. 31, no. 3, pp. 523–540, 2007.

[14] R. Yund, M. Blanpied, T. Tullis, and J. Weeks, "Amorphous material in high strain experimental fault gouges," *Journal of Geophysical Research*, vol. 95, no. B10, pp. 15589–15602, 1990.

[15] Y. Wang, B. Zhang, S. H. Gao, and C. H. Li, "Investigation on the effect of freeze-thaw on fracture mode classification in marble subjected to multi-level cyclic loads," *Theoretical and Applied Fracture Mechanics*, vol. 111, p. 102847, 2021.

[16] H. R. Nejati and A. Ghazvinian, "Brittleness effect on rock fatigue damage evolution," *Rock Mechanics and Rock Engineering*, vol. 47, no. 5, pp. 1839–1848, 2014.

[17] Y. Wang, B. Zhang, B. Li, and C. H. Li, "A strain-based fatigue damage model for naturally fractured marble subjected to freeze-thaw and uniaxial cyclic loads," *International Journal of Damage Mechanics*, vol. 30, no. 10, pp. 1594–1616, 2021.

[18] S. Zhang, W. Gao, L. Yan, J. Liu, and L. Liu, "The characteristics of blasting vibration frequency bands in jointed rock mass slope," *Environmental Earth Sciences*, vol. 79, no. 23, pp. 1–17, 2020.

[19] Y. Wang, Z. Cao, Z. Song, C. Zhu, and J. Han, "On fracture and damage evolution modelling of fissure-hole containing granite induced by multistage constant-amplitude variable-frequency cyclic loads," *Fatigue and Fracture of Engineering Materials and Structures*, vol. 133, pp. 1–17, 2022.

[20] R. Shirani Faradonbeh, A. Taheri, and M. Karakus, "Fatigue failure characteristics of sandstone under different confining pressures," *Rock Mechanics and Rock Engineering*, vol. 55, pp. 1–26, 2022.

[21] Y. Wang, H. N. Yang, J. Q. Han, and C. Zhu, "Effect of rock bridge length on fracture and damage modelling in granite containing hole and fissures under cyclic uniaxial increasing-amplitude decreasing-frequency (CUIADF) loads," *International journal of fatigue*, vol. 158, p. 106741, 2022.

[22] Y. Wang, J. Q. Han, Z. Y. Song, and C. Zhu, "Macro-meso failure behavior of pre-flawed hollow-cylinder granite under multi-level cyclic loads: insights from acoustic emission and post-test CT scanning," *Engineering Fracture Mechanics*, vol. 258, p. 108074, 2021.

[23] S. Ren, Y. M. Bai, J. P. Zhang, D. Y. Jiang, and C. H. Yang, "Experimental investigation of the fatigue properties of salt rock," *International Journal of Rock Mechanics and Mining Sciences*, vol. 64, pp. 68–72, 2013.

[24] Y. Wang, J. Li, C. Zhu, and T. Mao, "Fatigue failure identification using deformation and energy rate for hole-fissure contained granite under freeze–thaw and variable-frequency–variable-amplitude cyclic loads," *Fatigue & Fracture of Engineering Materials & Structures*, vol. 45, no. 3, pp. 834–851, 2022.

[25] Y. Liu, F. Dai, L. Dong, N. Xu, and P. Feng, "Experimental investigation on the fatigue mechanical properties of intermittently jointed rock models under cyclic uniaxial compression

with different loading parameters," *Rock Mechanics and Rock Engineering*, vol. 51, no. 1, pp. 47–68, 2018.

[26] H. Y. Zhang, W. J. Xu, and Y. Z. Yu, "Triaxial tests of soil–rock mixtures with different rock block distributions," *Soils and Foundations*, vol. 56, no. 1, pp. 44–56, 2016.

[27] H. Z. Wei, W. J. Xu, X. F. Xu, Q. S. Meng, and C. F. Wei, "Mechanical properties of strongly weathered rock-soil mixtures with different rock block contents," *International Journal of Geomechanics*, vol. 18, no. 5, p. 04018026, 2018.

[28] H. Sonmez, C. A. N. D. A. N. Gokceoglu, E. W. Medley, E. R. G. Ü. N. Tuncay, and H. A. Nefeslioglu, "Estimating the uniaxial compressive strength of a volcanic bimrock," *International Journal of Rock Mechanics and Mining Sciences*, vol. 43, no. 4, pp. 554–561, 2006.

[29] A. Y. C. A. N. Kalender, H. Sonmez, E. Medley, C. Tunusluoglu, and K. E. Kasapoglu, "An approach to predicting the overall strengths of unwelded bimrocks and bimsoils," *Engineering Geology*, vol. 183, pp. 65–79, 2014.

[30] S. Kahraman, M. Alber, M. Fener, and O. Gunaydin, "An assessment on the indirect determination of the volumetric block proportion of Misis fault breccia (Adana, Turkey)," *Bulletin of Engineering Geology and the Environment*, vol. 74, no. 3, pp. 899–907, 2015.